Research Article

Cluster-model-embedded first-principles study of thermodynamic stability and elastic properties in (Zr, Ti)C_x carbides

Qixiang Zhang[1], Zhen Li[2,*], Ben Niu[1], Qing Wang[1,*], Chuang Dong[1], Zhongwei Zhang[3,*]

[1]School of Materials Science and Engineering, Dalian University of Technology, Dalian 116024, Liaoning, China.
[2]School of Mechanical Engineering, Dalian University of Technology, Dalian 116024, Liaoning, China.
[3]Institute of Advanced Structure Technology, Beijing Institute of Technology, Beijing 100081, China.

[*]**Correspondence to:** Prof. Zhen Li, School of Mechanical Engineering, Dalian University of Technology, Dalian 116024, Liaoning, China. E-mail: lizhen@dlut.edu.cn; Prof. Qing Wang, School of Materials Science and Engineering, Dalian University of Technology, Dalian 116024, Liaoning, China. E-mail: wangq@dlut.edu.cn; Prof. Zhongwei Zhang, Institute of Advanced Structure Technology, Beijing Institute of Technology, Beijing 100081, China. E-mail: 6120190123@bit.edu.cn

How to cite this article: Zhang Q, Li Z, Niu B, Wang Q, Dong C, Zhang Z. Cluster-model-embedded first-principles study of thermodynamic stability and elastic properties in (Zr, Ti)C_x carbides. *J Mater Inf* 2026;6:[Accept]. http://dx.doi.org/10.20517/jmi.2025.82

Received: 29 September 2025 | **Revised:** 25 November 2025 | **Accepted:** 22 December 2025

Abstract

Multi-component carbide ceramics have garnered significant attention as ultra-high-temperature structural materials due to their exceptionally high melting points and

excellent mechanical properties. In this work, we systematically investigate the synergistic effects of C vacancies and Ti alloying on the thermodynamic stability and elastic behavior of (Zr, Ti)C_x carbides using first-principles calculations. Specific cluster structural models of [C-M_6](C,□)$_5$ (M = Zr/Ti, □ = vacancy) were constructed by considering the local chemical short-range orders of elemental distribution and the ordering of vacancies on C sublattice, which were then employed as inputs for first-principles calculations. The results reveal that the introduction of C vacancies decreases the free energy at high temperatures and enhances the thermodynamic stability, whereas Ti substitution for Zr tends to reduce stability. Notably, the ternary carbide $Zr_5Ti_1C_5$ ([C-Zr_5Ti_1](C,□)$_5$) with an equimolar ratio of Ti-to-vacancy ratio of exhibits an superior high-temperature thermodynamic stability. Analysis of entropy contributions indicates that both vacancies and Ti addition primarily alter the free energy by modifying the lattice vibration modes, an effect dominated by the vibrational entropy. These two types of defects weaken the M-C bond strength, resulting in reduced binding energy and Young's modulus. Furthermore, this synergistic effect considerably lowers the critical temperature required to stabilize the single-phase solid solution structure in multi-component carbides, which is attributed to a decrease in mixing enthalpy and an increase in configurational entropy caused by vacancies. The cluster-model-embedded first-principles approach offers valuable insight for designing high-performance carbides in complex ceramic systems.

Keywords: First-principles calculations, MC carbides, cluster model, free energy, Young's modulus

INTRODUCTION

Carbide ceramics composed of transition metals (TMs) have shown broad application prospects in aerospace and high-temperature (HT) structural materials due to their ultra-high melting points (> 3273 K), and excellent chemical stability[1-4]. Among them, ZrC (FCC-NaCl type) has been widely used in wear-resistant coatings, high-speed cutting tools, and HT ceramic components owing to its high Young's modulus (464 ± 22 GPa), high hardness (25.2 ± 1.4 GPa), and high thermal conductivity (33.5 W/(m·K))[5,6]. However, binary carbides are susceptible to carbon volatilization and lattice degradation at HTs, leading to a significant reduction in their load-bearing capacity[7-9]. To address these limitations, multi-element alloying has been widely adopted to enhance the

thermodynamic stability and elastic modulus of carbides by introducing lattice distortion and modulating valence electron concentration (VEC)[10-12]. For example, the high-entropy carbide (TaHfZrNb)C with an equi-molar mixing of TMs demonstrates excellent thermal stability and HT creep resistance compared to binary carbides[13], which is attributed to its lattice distortion and entropy stabilization effects. Notably, its steady-state creep rate (~ 1.36×10^{-8} s^{-1}) is an order of magnitude lower than those of ZrC (~ 2.3×10^{-7} s^{-1}) and NbC (~ 1.56×10^{-7} s^{-1})[13]. Similarly, the single-phase high-entropy $(Hf_{0.2}Zr_{0.2}Ta_{0.2}Nb_{0.2}Ti_{0.2})C$ carbide exhibits a higher elastic modulus (~ 520 GPa) than its binary counterparts (e.g., ZrC: 464 GPa, HfC: 352 GPa, TaC: 409 GPa), which results from enhanced solid-solution strengthening due to the severe lattice distortion in high-entropy alloys[14]. Moreover, the vacancies in C sublattice have also emerged as an effective means of performance regulation[15]. The highest melting point of binary MC-type carbides often appears in the metal-rich region rather than at stoichiometry, suggesting that the vacancies can enhance HT stability[16]. Furthermore, the elastic modulus (~ 660 GPa) of non-stoichiometric $(VNbTaMoW)_{0.5}C_{0.4}$ carbide significantly exceeds that (~ 570 GPa) of its stoichiometric analogue, further underscoring the beneficial role of C-side vacancies[17]. These findings imply that the synergistic effects between carbon vacancies and multi-metal cations can significantly improve both thermodynamic stability and elastic properties. Nevertheless, systematic studies and mechanistic insights into the role of C-vacancy content in multi-component carbides remain scarce.

Although experimental studies have demonstrated the advantages of vacancies and multi-element alloying in MC-type carbides, the intrinsic mechanisms governing thermodynamic stability are still unclear, largely due to the challenges in experimental characterization with sufficient accuracy. In recent years, first-principles calculations based on density functional theory (DFT) have become essential for atomic-level design and mechanistic exploration of material properties[18-20]. For instance, the Cluster Expansion Method (CEM) studies have revealed that the formation energy of ordered carbon vacancies in ZrC_x is lower than that of disordered ones at 0 K, indicating superior stability of ordered configurations[21]. Research on $(Ti_{1-y}Ni_y)C_x$ ternary carbides using special quasi-random structure (SQS) method shows that the thermodynamic stability increases with C-vacancy concentration, and that high Ni content necessitates the

presence of vacancies[22,23]. However, computational investigations into the ordered vacancies and chemical short-range orders (CSROs) in multi-component carbides are still limited. Conventional modeling approaches, such as SQS and supercell methods, were employed to construct the solid-solution structures of multi-component carbides, but often struggle to accurately capture ordered vacancy distribution and local chemical environments[24,25]. These methods also require large supercells for multi-component systems[26,27], leading to high computational costs that impede efficient screening and analysis. Therefore, there is a critical need for computational models capable of effectively representing ordered C-vacancies and incorporating CSROs to enable accurate theoretical insights into the thermodynamic stability and property modulation mechanisms of multi-component carbides.

In previous work, we developed a cluster-plus-glue-atom model to describe the CSROs in multi-component solid-solution alloys[28-30], providing a reliable approach to consider the interactions among multiple elements. Herein, we extend this model to the MC-type carbides. A series of structural models, encompassing binary (ZrC, Zr_6C_5, Zr_3C_2) and ternary ($Zr_5Ti_1C_6$, $Zr_5Ti_1C_5$, $Zr_5Ti_1C_4$, $Zr_4Ti_2C_6$, $Zr_4Ti_2C_5$) carbides, will be constructed by systematically varying metal species (M = Zr, Ti) and C vacancy concentrations, with the ordered arrangement of C vacancies explicitly incorporated. These periodic cluster-based models will serve as input for first-principles calculations to determine equilibrium lattice constants, binding energy, formation energy, free energy, and HT elastic modulus, thereby elucidating the cooperative effect of vacancy concentration and Ti alloying on thermodynamic stability and elastic properties. Further analysis of entropy, electronic density of states, and phonon density of states will reveal the dominant factors governing free energy, bonding characteristics, and dynamical stabilities. Finally, the key factors affecting the formation of single-phase solid solution will be identified by evaluating the free energy change associated with the formation of (Zr, Ti)C_x from binary ZrC_x and TiC_x.

MATERIALS AND METHODS

First principles calculations

Construction of cluster structural models

It is well known that vacancies in non-stoichiometric carbides are not randomly distributed[31]. Experimentally confirmed in systems such as ZrC_x, TiC_x, and NbC_x ($x < 1$), the ordered arrangement of vacancies on the C sublattice is considered

thermodynamically stable at room temperature (RT)[32-35]. Computational studies further reveal that chemical bonding in multi-component carbides is highly localized, occurring mainly between central atoms and their first- and second-nearest neighbors[36]. Therefore, these systems can be effectively represented by a cluster-plus-glue-atom structural model that reflects the coordination environment of the central atom over two nearest neighbors[28]. In this model, the cluster is defined as a coordination polyhedron comprising a central solute atom surrounded by its nearest-neighbor solvent atoms, where the strong interaction between them gives rise to the strongest CSRO. And other solute atoms having weaker interactions with the base serve as the glue atoms, occupying the inter-cluster sites to mediate atomic packing. The resulting structural unit is expressed as [cluster](glue atom)$_m$, where m denotes the number of glue atoms per cluster. For MC-type solid solution carbides, the vacancies are located at the glue atom sites to ensure the integrity of the cluster structural unit since vacancies can generally be originated on the C side. Then, the cluster structural unit centered on C, with metal M atoms as shell atoms and the remaining C atoms and vacancies (C/□) serving as glue atoms are constructed. The cluster usually adopts an octahedron with a coordination number of CN = 6 (coordination number = 6), composed of a central C atom (marked by green sphere in Figure 1A) and six M atoms (blue spheres) in the first coordination shell. The second-nearest-neighbor sites around the central C atom (gray spheres in Figure 1A) serve as the glue atom sites, which are occupied by C or □. To preserve the crystal periodicity and stoichiometry of the ideal MC structure (M : C = 1 : 1), each [C-M$_6$] cluster has five such sites, resulting in the cluster formula [C-M$_6$](C,□)$_5$, marked by red sphere in Figure 1B-F).

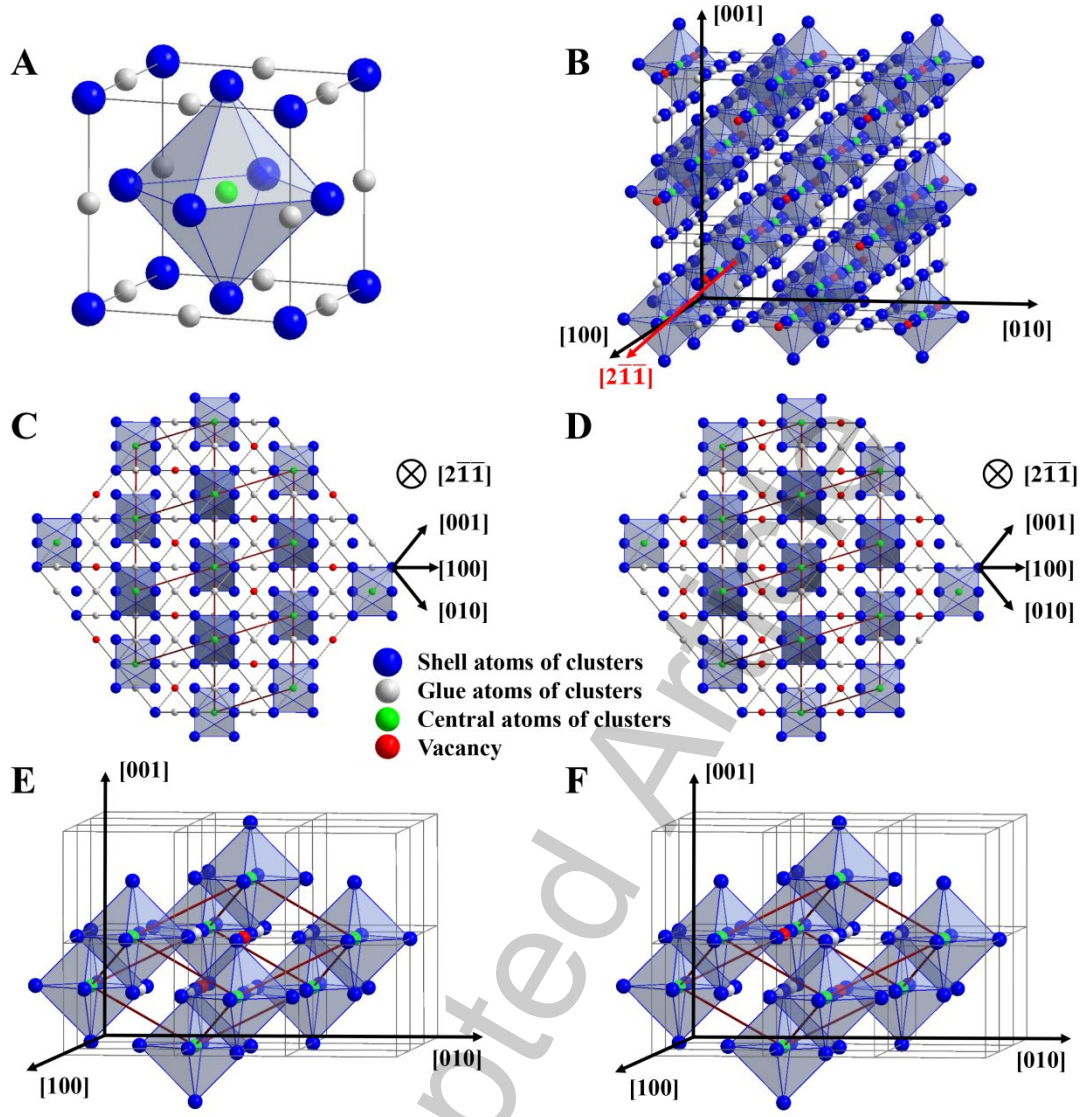

Figure 1. Cluster-glue-atom model in MC-type carbides. (A) Atomic structure of ZrC structure, showing that the CN6 cluster polyhedron is centered by a C atom (green sphere) and surrounded by six metal atoms (blue spheres); (B) Vacancy-ordered structure extracted from a 3×3×3 supercell of MC, showing the vacancy channels along the [$2\bar{1}\bar{1}$] direction; (C, D) Derived cluster units for M_6C_5 and M_6C_4, illustrating the arrangement of vacancies within the channel framework; (E, F) Three-dimensional periodic supercells of M_6C_5 and M_6C_4, constructed by the stacking of cluster units shown in Figure 1C and D. The cluster models were generated using the Visualization for Electronic and Structural Analysis (VESTA) software

Since the introduction of specific vacancy sequences in the C sublattice has been shown to improve the structural stability[15,32], this study focuses on two C-deficient compositions, M_6C_5 and M_6C_4 (= M_3C_2). Guided by the ordered vacancy-channel

distribution reported in the literature[37], the atomic structures of these carbides were reconstructed with a 3×3×3 supercell (Figure 1B). Vacancy channels are clearly visible along the $[2\bar{1}\bar{1}]$ direction of the MC lattice, where the vacancies occupy the second-nearest neighbor sites around the central C atom. Figure 1C and D show the vacancy channel distributions for M_6C_5 and M_3C_2, respectively, along this direction. In the M_6C_5 structure (Figure 1C), the C sublattice consists of two alternating layer types: one with two-thirds of sites occupied by C atoms and one-third forming vacancy rows, creating a channel-like structure, and the other fully occupied by C. In M_3C_2 containing a higher vacancy concentration (Figure 1D), the vacancy channel is more prominent: the first layer contains only one-third C rows and two-thirds vacancy rows, while the second layer is fully C-occupied.

Then, a periodic structural unit containing 12 sites (including vacancies), which fully incorporates the cluster model information, can be identified from the brown boxes in Figure 1C and D. Its composition corresponds exactly to the cluster formula $[C\text{-}M_6](C,□)_5$. The extracted structural units in three-dimension space are displayed in Figure 1E and F. The basis vectors (X, Y, Z) of the supercell are aligned with the [211], $[\bar{1}2\bar{1}]$, and $[\bar{2}11]$ directions of the original FCC lattice, respectively. And the lattice parameters are $a=b=c=\sqrt{6}/2a_0$, with angles □ = 60°, □ = 109.47°, and γ = 99.59°, where a_0 denotes the lattice constant of original FCC structure. In this supercell, the vertex positions are occupied by C atoms, which acts as the central atoms of clusters, while the six metal atoms of the cluster shell and five glue atoms (C atoms and vacancies) reside within the supercell. Detailed atomic coordinates are listed in Supplementary Table 1.

It is noted that in the localized cluster model for MC metal carbides, both the M and C sublattices still maintain a complete NaCl-type lattice structure. Moreover, C occupies the center site of the cluster model, thereby guaranteeing that the glue atom site is occupied only by C/□ rather than metal atoms. Based on this model and previous evidence that Ti interacts more strongly with vacancies than Zr[38], Ti atoms were placed near C vacancies in the current model. To systematically evaluate the influence of Ti content and vacancy concentration on the structure and properties of carbides, the supercell structures corresponding to these designed carbide compositions are illustrated in Supplementary Figure 1.

Calculation methods

The first-principles DFT calculations were performed using the plane-wave (PW) basis set and projector-augmented wave (PAW) method, as implemented in the Vienna ab initio Simulation Package (VASP)[39-41]. The electronic exchange-correlation potential was described within the generalized-gradient approximation (GGA) using the Perdew-Burke-Ernzerhof (PBE) parameterization[42]. The C-$2s^2 2p^2$, Ti-$3p^6 3d^2 4s^2$, and Zr-$4s^2 4p^6 5s^2 4d^2$ were treated as the valence states. The kinetic energy cutoff of 800 eV was employed for the plane-wave basis. Ionic positions and lattice parameters of cluster structural models were fully relaxed during the geometrical optimization, with convergence criteria set to a Hellmann-Feynman force tolerance below 0.02 eV $Å^{-1}$ and an energy tolerance of 1×10^{-8} eV. Γ-centered k-point meshes with a spacing of 0.02 $Å^{-1}$ were generated according to the Monkhorst-Pack scheme for all calculations. All structural models were built and visualized using the Visualization for Electronic and Structural Analysis (VESTA) software[43], and the electronic density of states was calculated using VASPKIT toolkit[44].

The formation energy (E_f) and binding energy (E_b) of each carbide were calculated using the fundamental physical expressions of Equation (1) and (2):

$$E_f = (E_{tot} - \sum E_M)/n \quad (1)$$

$$E_b = (E_{tot} - \sum E_{single})/n \quad (2)$$

where E_f represents the energy required to form the carbide structure, defined as the difference between the total energy of the optimized structure (E_{tot}) and the sum of the energies of individual atoms in their standard elemental states (E_M), n is the total number of atoms. For Zr and Ti, their standard states are the hexagonal close-packed (HCP) structure with the space group of $P6_3/mmc$, while the carbon adopts the graphite structure with the same space group. The DFT-D3 dispersion correction[45] is applied to accurately describe the interlayer van der Waals interactions in graphite. E_b reflects the energy associated with atomic bonding relative to isolated states (E_{single}). The ideal single-atom energy (E_{single}), i.e., the energy of an isolated atom, is calculated by placing a single atom in a large supercell with a lattice constant of 15 Å to minimize the interactions among

periodic images.

To assess the temperature-dependent stability, the Helmholtz free energy $F(T)$ of carbide was computed as[46]:

$$F(T) = E_{tot} + F_{el}(T) + F_{vib}(T) + F_{mag}(T) - TS_{conf} \quad (3)$$

where $F_{vib}(T)$, $F_{el}(T)$, $F_{mag}(T)$, and S_{conf} represent the vibrational, electronic, and magnetic free energies, and configurational entropy, respectively. As the system is non-magnetic, F_{mag} = 0. Lattice dynamics calculations and related thermodynamic properties (free energy and entropy) were performed using the finite displacement method. Supercells with lattice constants larger than 9 Å were built to avoid spurious self-interactions, where each atom was displaced by 0.01 Å along the three Cartesian directions. Force constants were obtained via finite differences, and phonon frequencies were Fourier-interpolated to a 25×25×25 q-point grid using the phonopy package[47]. The resulting force-constant matrices were subsequently utilized to compute the thermodynamic properties of carbides. Thermodynamic quantities were evaluated within the harmonic approximation up to 2000 K. The vibrational free energy and vibrational entropy were derived from phonon calculations, as follows[48]:

$$F_{vib} = \frac{1}{2} \sum_{q,v} \hbar\omega_{q,v} + k_B T \sum_{q,v} \ln\left[1 - exp\left(-\hbar\omega_{q,v}/k_B T\right)\right] \quad (4)$$

$$S_{vib} = -k_B \sum_{q,v} \ln\left[1 - exp\left(-\hbar\omega_{q,v}/k_B T\right)\right] - \frac{1}{T}\sum_{q,v} \frac{\hbar\omega_{q,v}}{exp\left(-\hbar\omega_{q,v}/k_B T\right)-1} \quad (5)$$

where k_B is Boltzmann constant, q is the wave vector, v denotes the phonon mode index, $\omega_{q,v}$ represents the phonon frequency at the wave vector modes q and v, T is the absolute temperature, and $\hbar$ is the reduced Planck constant. The electronic free energy and electronic entropy are expressed with Equations (6-8)[49]:

$$F_{elec} = U_{elec} - TS_{elec} \quad (6)$$

$$U_{elec} = \int_{-\infty}^{\infty} n(\varepsilon) f(\varepsilon, T) \varepsilon d\varepsilon - \int_{-\infty}^{\varepsilon_f} n(\varepsilon) \varepsilon d\varepsilon \quad (7)$$

$$S_{elec} = -k_B \int_{-\infty}^{\infty} n(\varepsilon)\left[f(\varepsilon, T) \ln f(\varepsilon, T) + \left(1 - f(\varepsilon, T)\right) \ln(1 - \ln(\varepsilon, T))\right] \varepsilon d\varepsilon \quad (8)$$

where $n(\varepsilon)$ is the electronic density of states, ε_f is the Fermi energy, and $f = f(\varepsilon, T)$ is the Fermi-Dirac distribution function. The configurational entropy S_{conf} is calculated using Equation (9)[50]:

$$S_{conf} = -R[\frac{X}{X+Y}\sum_{i=1}^{N_h} x_i^h \ln(x_i^h) + \frac{Y}{X+Y}\sum_{i=1}^{N_k} x_i^k \ln(x_i^k)] \quad (9)$$

where the sublattice h contains X sites and sublattice k contains Y sites; R is the ideal gas constant; N_h and N_k are the number of element types in sublattices h and k, respectively. x_i^h and x_i^k are molar fractions of component i in each sublattice.

The elastic modulus of carbide at 0 K was computed from the stress-strain relationship[51,52]. For the crystal symmetries, VASP generated the necessary strain configurations, where strains with magnitudes of ±1% and ±2% were applied along the relevant Cartesian directions in both tensile and compressive sense for each component. Its high-temperature behavior was approximated using the empirical function proposed by Zakarian et al.[53]:

$$\frac{E(T)}{E_0} = 1 - 0.2\left(\frac{T}{T_{max}}\right) - 0.25\left(\frac{T}{T_{max}}\right)^2 \quad (10)$$

where E_0 is the elastic modulus at 0 K from DFT, T_{max} is the melting temperature calculated from the CALPHAD method[54,55]. Thus, $E(T)$ can be determined for any temperature given E_0 and T_{max}.

RESULTS AND DISCUSSION

Formation and binding energies of (Zr, Ti)-C carbides

To validate the selected computational parameters and the accuracy of the cluster model, the calculated lattice constants of Zr-based carbides were compared with available experimental data. The DFT-calculated lattice constant of stoichiometric ZrC is a = 4.710 Å, showing excellent agreement with the experimental values of 4.692 ~ 4.705 Å[56,57]. With the introduction of C vacancies, the lattice constant of Zr_6C_5 (C/Zr = 0.83) increases to a = 4.719 Å, consistent with the reported value of 4.702 Å[58]. This expansion is attributed to the Coulomb repulsion between excess electrons localized at vacancy

sites[59], leading to a local lattice distortion and an overall increase in the lattice constant. Upon Ti doping, the lattice constant decreases to a = 4.664 Å for $Zr_5Ti_1C_5$, due to the smaller atomic radius of Ti (1.47 Å) compared to Zr (1.60 Å). This result agrees well with the reported value (~ 4.633 Å) of $(Zr_{0.8}Ti_{0.2})C_{0.8}$[60].

The structural stability of designed carbides was evaluated by calculating their formation energy E_f and binding energy E_b, as shown in Figure 2. ZrC exhibits the most negative formation energy (E_f = -0.786 eV/atom), indicating the highest stability at 0 K. The introduction of one C vacancy in Zr_6C_5 raises the formation energy to E_f = -0.782 eV/atom, while Zr_3C_2 containing two vacancies shows a further increase to -0.721 eV/atom, demonstrating that the carbon vacancies reduce the low-temperature stability of ZrC. Similarly, the Ti alloying destabilizes the carbide structure since $Zr_5Ti_1C_6$ (E_f = -0.743 eV/atom) and $Zr_4Ti_2C_6$ (E_f = -0.721 eV/atom) are less stable than ZrC (Figure 2A). However, the effect of vacancies on structural stability is not monotonic in Ti-containing carbides. $Zr_5Ti_1C_5$ exhibits a more negative E_f (-0.746 eV/atom) than $Zr_5Ti_1C_6$ (-0.743 eV/atom), whereas $Zr_5Ti_1C_4$ (with two vacancies) is significantly less stable (E_f = -0.697 eV/atom) (Figure 2B). This suggests that Ti promotes the formation of local C vacancies, and a moderate non-stoichiometry enhances the local atomic relaxation and charge transfer, leading to a localized strengthening effect[61]. The phenomenon is also observed in TiC_x, where Ti_6C_5 (E_f = -0.776 eV/atom) exhibits a higher structural stability than stoichiometric TiC (E_f = -0.750 eV/atom) (Table S2), consistent with the C vacancy stabilization reported by Kim et al[62]. Furthermore, the binding energy (E_b) increases with C vacancy concentration and Ti addition (Figure 2), indicating the weakened M-C bonding due to the reduced coordination near vacancies and Ti-induced lattice distortion.

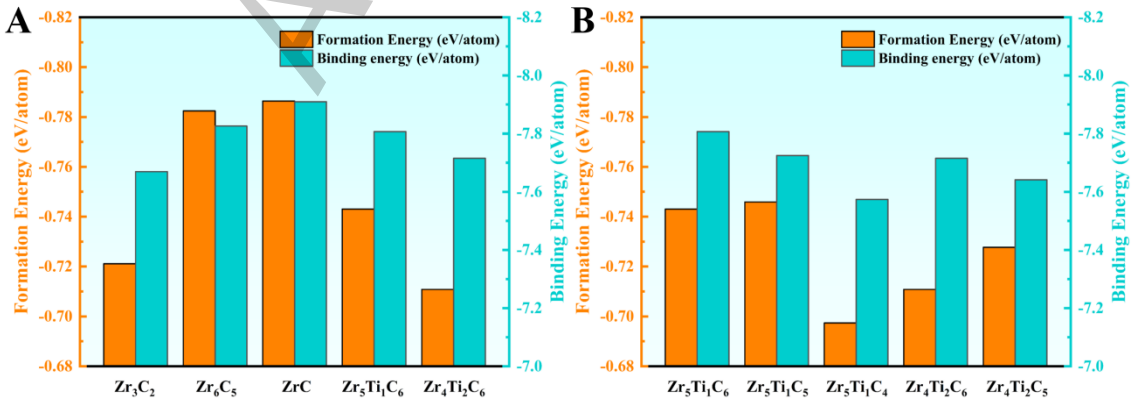

Figure 2. Formation energy (orange y-axis) and binding energy (cyan y-axis) of (Zr, Ti)-

C carbides. (A) Zr_3C_2, Zr_6C_5, ZrC, $Zr_5Ti_1C_6$, and $Zr_4Ti_2C_6$ with different stoichiometric ratios; (B) $Zr_5Ti_1C_6$, $Zr_5Ti_1C_5$, $Zr_5Ti_1C_4$, $Zr_4Ti_2C_6$, and $Zr_4Ti_2C_5$ by varying the concentrations of Ti and vacancies.

Free energies of (Zr, Ti)-C carbides

Since the formation energy reflects the structural stability at 0 K alone, the Helmholtz free energy (*F*) was computed to evaluate the thermodynamic stability of carbides at elevated temperatures. Figure 3 shows the temperature dependence of free energy from 0 K to 2000 K, indicating a decrease in free energy with rising the temperature for all carbides. For the binary Zr-C carbides, the introduction of C vacancies reduces the stability at low temperatures, as evidenced by the fact that ZrC has a lower free energy than Zr_6C_5 below 1131 K. Above this temperature, the stability order reverses, with Zr_6C_5 becoming more stable than ZrC. For Zr_3C_2 containing two vacancies, the transition temperature for structural stability exceeds 2000 K.

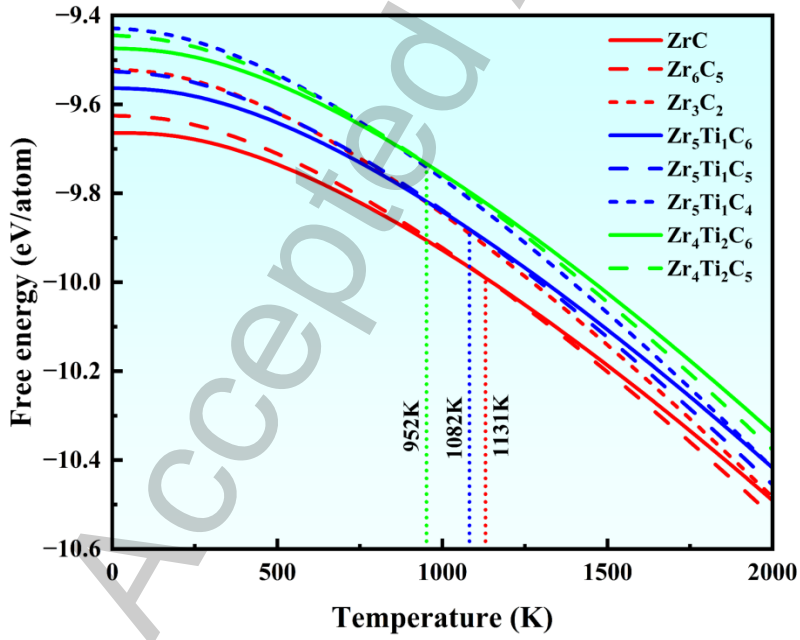

Figure 3. Helmholtz free energy as a function of temperature for (Zr, Ti)-C carbides

In ternary (Zr, Ti)-C carbides, the free energy increases with Ti content (solid lines in Figure 3), indicating that the substitution of Ti for Zr reduces the thermodynamic stability. C vacancies also induce a stability inversion in these carbides, but the transition temperature decreases with higher Ti content: from 1131 K for ZrC-Zr_6C_5 pair to 1082 K for $Zr_5Ti_1C_6$-$Zr_5Ti_1C_5$ and 952 K for $Zr_4Ti_2C_6$-$Zr_4Ti_2C_5$ (blue and cyan curves in Figure 3). This indicates that Ti addition preferentially stabilizes the M_6C_5 structure over the

M_6C_6 at high temperatures. However, excessive C vacancies are detrimental, as $Zr_5Ti_1C_4$ exhibits higher free energy than $Zr_5Ti_1C_5$ across the entire temperature range. Therefore, $Zr_5Ti_1C_5$, with a specific combination of one C vacancy and one Ti atom, demonstrates an optimal HT stability due to the synergistic effect of vacancy and metal alloying. It should be noted that the present free energy trends are evaluated from 0 K to 2000 K. Extrapolation to ultra-high temperatures (> 2500 K) may involve additional contributions such as anharmonic lattice softening, phase transitions, or decomposition[8], which are beyond the scope of the current model and should be considered in further high-temperature assessments.

Elastic properties of (Zr, Ti)-C carbides

Elastic properties, particularly Young's modulus, are critical indicators for ultra-high-temperature structural materials, as they reflect the bonding strength and structural integrity. The temperature-dependent Young's moduli of carbides were calculated using first-principles results combined with the empirical model proposed by Zakarian et al[53], as shown in Figure 4. It is found that the modulus decreases with the temperature due to the weakening of interatomic bonds by thermal vibrations. To validate the model, compositions close to the experimentally-studied $ZrC_{0.96}$ and $ZrC_{0.85}$ were selected due to the scarcity of HT elastic data for carbides. The calculated moduli of ZrC and Zr_6C_5 agree well with available experimental and theoretical data[63,64]. Both calculations and experiments confirm that increasing C vacancy concentration significantly reduces the Young's modulus. Although vacancies may enhance the local M-M bonding, the overall reduction in bond density due to missing C atoms diminishes the material's resistance to elastic deformation. Ti-containing $Zr_5Ti_1C_6$ and $Zr_4Ti_2C_6$ exhibit lower Young's modulus than pure ZrC across the temperature range, which is attributed to the weaker bonding strength of Ti-C compared to Zr-C, leading to reduced stiffness. Notably, $Zr_5Ti_1C_5$ maintains a slightly higher modulus than $Zr_4Ti_2C_5$ at HTs, indicating superior HT structural stability, consistent with the free energy trends. Within the studied temperature range (below 2000 K), the stable-lattice approximation provides a solid basis for interpreting the elastic properties, while beyond this range would necessitate accounting for additional factors such as lattice softening and carbon evaporation.

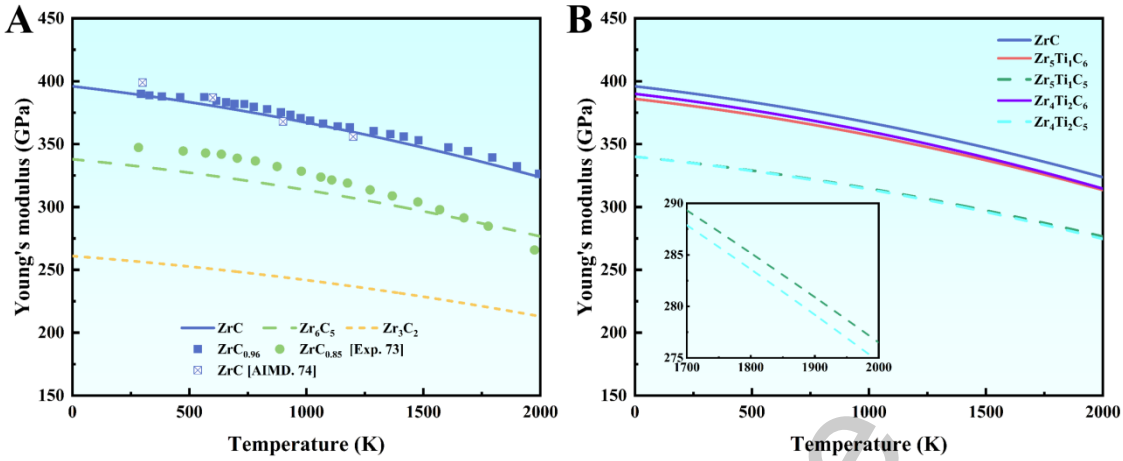

Figure 4. Young's modulus as a function of temperature for ZrC_x in Figure 4A and (Zr, Ti)C_x series of carbides in Figure 4B, where scattered points represent experimental data, and solid lines denote corresponding theoretical fittings.

Thermodynamic stability of designed (Zr, Ti)-C carbides

The above results reveal that the introduction of vacancies leads to an intersection in the free energy curves at HTs, resulting in a stability transition, whereas the substitution of Ti for the base Zr raises the free energy and reduces the thermodynamic stability of (Zr,Ti)-C ternary carbides (Figure 3). To further elucidate the influence of vacancies and Ti addition on free energy, Figure 5 and Supplementary Figure 2(A, B) present the entropy contributions in the designed different carbides as a function of temperature. The results show that the vibrational entropy (S_{vib} = 0 ~ 8 k_B/atom) dominates the free energy at elevated temperatures, compared to the electronic entropy (S_{el} = 0 ~ 0.6 k_B/atom) and configurational entropy (S_{conf} = 0 ~ 0.28 k_B/atom). Moreover, the C vacancies increase all entropy components (Figure 5), thereby lowering the free energy and enhancing the thermodynamic stability. This is the primary reason for the stability transition observed in vacancy-containing carbides at HTs. In contrast, the Ti addition reduces the vibrational entropy while increasing the configurational entropy, with a negligible impact on electronic entropy (Figure 5B). Given the dominant role of vibrational entropy, the net effect of Ti alloying in an increase in the overall free energy, consistent with the trends shown in Figure 3.

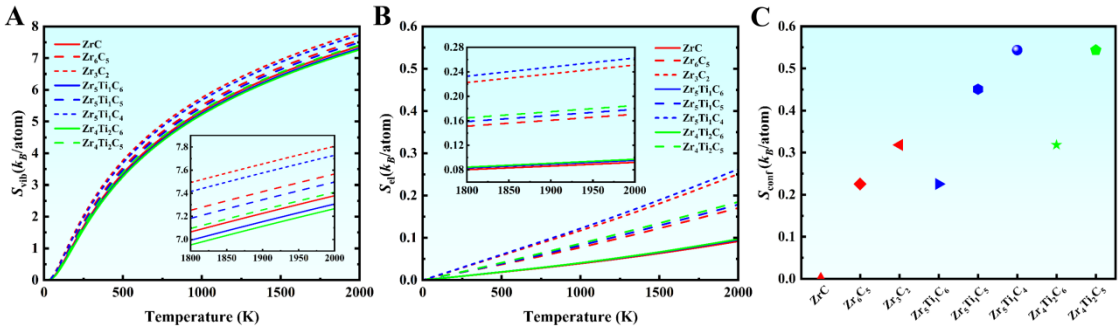

Figure 5. Contributions to the total entropy as a function of temperature for (Zr, Ti)C_x carbides. (A) Vibrational entropy; (B) Electronic entropy; (C) Configurational entropy.

For the dominant vibrational entropy, it originates from lattice vibrations, and its magnitude is directly governed by the phonon density of states (PhDOS), as presented in Figure 6A-C and Supplementary Figure 2C, displaying the PhDOSs of the designed carbides. The absence of imaginary frequencies in PhDOSs of all binary and ternary carbides confirms their dynamic stability. For binary ZrC, phonon modes are distributed between 0 ~ 9.9 THz and 12.5 ~ 19.9 THz (Figure 6A). Introducing the C vacancies causes the low-frequency vibration modes in Zr_6C_5 and Zr_3C_2 to extend to lower frequencies, while the high-frequency range contracts. This shift results from the lattice relaxation induced by C vacancies, i.e., the localized structural softening enhances low-frequency vibrations, whereas the loss of C atoms diminishes high-frequency modes associated with C vibrations, leading to a contraction in the high-frequency region. Since the low-frequency vibrations contribute more significantly to vibrational entropy than high-frequency modes[65], C vacancies enhance the thermodynamic stability of carbides. Also, the Ti addition also affects the lattice vibrations markedly, as seen in Figure 6B and Supplementary Figure 4. Ti addition shifts the Zr-dominated acoustic peaks toward higher frequencies, thereby reducing the low-frequency phonon proportion in $Zr_5Ti_1C_6$ and $Zr_4Ti_2C_6$, owing to its lower atomic mass (Ti: 49 amu, Zr: 91 amu) and higher vibration frequency[66]. Consequently, excessive Ti addition reduces the thermodynamic stability due to the entropy loss and lattice distortion.

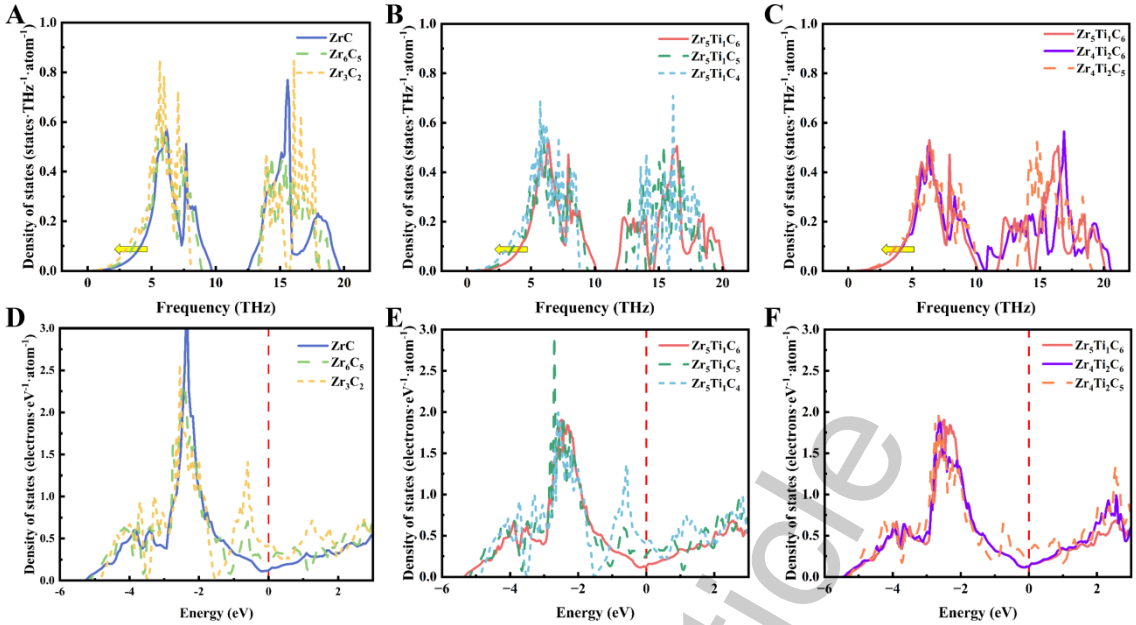

Figure 6. Density of states analysis for (Zr, Ti)C_x carbides. (A-C) Phonon density of states probing lattice dynamics; (D-F) Electronic density of states revealing electronic structure.

Moreover, the electronic density of states (DOS) in the designed carbides are also presented in Figure 6D-F to further clarify the effects of vacancies and Ti addition on the thermodynamic stability. Analysis of the total and partial density of states (TDOS and PDOS; see Figure 6D-F, Supplementary Figure 2D and Supplementary Figure 3) shows a non-zero DOS at the Fermi level (set to zero and marked by a vertical dashed line) for all carbides, confirming their metallic bonding character. Compared with the ZrC, the covalent-character-dominated TDOS peaks decrease considerably in Zr_6C_5 and Zr_3C_2 (Figure 6D), indicating weakened bonding interactions between C-p and Zr-d orbitals and a corresponding reduction in M-C bond strength. A new hybridization peak emerges near ~ -0.8 eV, attributed to the rearrangement of local electronic structure caused by C vacancies, which promotes Zr-Zr metallic bonding near vacancy sites. Furthermore, the increased DOS at the Fermi level implies enhanced metallicity and weaker bonding strength. Figure 6E-F further reveal that the intensity of C-p and Zr/Ti-d hybridization peaks decreases with higher Ti content, suggesting that the Ti substitution for Zr also weakens bonding strength and undermines structural stability. The evolution of the electronic structure elucidated by DOS analysis clarifies the origin of bond weakening due to both C vacancies and increased Ti content. This weakening leads to a higher binding energy and a decreased Young's modulus, consistent with the trends observed in

Figures 2 and 4.

Formation of single-phase solid solution in multi-component carbides

The strong covalent bonding in carbides presents a formidable obstacle to the direct formation of single-phase FCC solid solution structure in multi-component systems from their binary counterparts. Therefore, the ability to form a single phase is a key indicator for evaluating the thermodynamic stability of multi-component carbides. The single-phase formability of (Zr, Ti)C_x was assessed by calculating the free energy change (ΔF) associated with its formation from binary ZrC_x and TiC_x, as defined in Equation (11):

$$\Delta F(y,x,T) = F\left(Zr_{6-y}Ti_yC_x,T\right) - \frac{(6-y)}{6}F(Zr_6C_x,T) - \frac{y}{6}F(Ti_6C_x,T) \quad (11)$$

where y is the number of Ti atoms in the M_6C_6 metal sublattice, x is the number of C atoms, and T is the temperature. Figure 7A shows the temperature dependence of ΔF for multi-component carbides. At low temperatures, ΔF is positive for all carbides, suggesting that (Zr, Ti)C_x is unstable and difficult to form as a stable single-phase solid solution. As the temperature increases, ΔF decreases and eventually becomes negative, indicating the formation single-phase solid solution becomes feasible. For instance, $Zr_5Ti_1C_6$ achieves the thermodynamic stability ($\Delta F < 0$) above 1663 K. With one C vacancy, $Zr_5Ti_1C_5$ stabilizes above 1489 K, and with two vacancies, $Zr_5Ti_1C_4$ stabilizes above 1041 K, demonstrating that C vacancies significantly reduces the formation temperature. These computational results align well with existing experimental observations[60]. For instance, stoichiometric $Zr_{0.8}Ti_{0.2}C_{1.0}$ failed to form a complete solid solution at 1873 K, whereas non-stoichiometric (Zr, Ti)C_x (x = 0.7 ~ 0.9) readily forms a single-phase FCC structure, confirming the beneficial role of vacancies in promoting the formation of single-phase solid solution. Furthermore, a higher Ti content raises ΔF of multi-component carbides, necessitating increased synthesis temperature. Compared to low-Ti $Zr_5Ti_1C_6$, the synthesis temperature for $Zr_4Ti_2C_6$ increases to 1758 K, indicating greater synthesis difficulty. This trend is consistent with experimental reports that higher Ti content complicates the synthesis[67,68]. However, introducing C vacancies substantially lowers the synthesis temperature, as in $Zr_4Ti_2C_5$, where it drops to 1515 K, thereby facilitating the synthesis process.

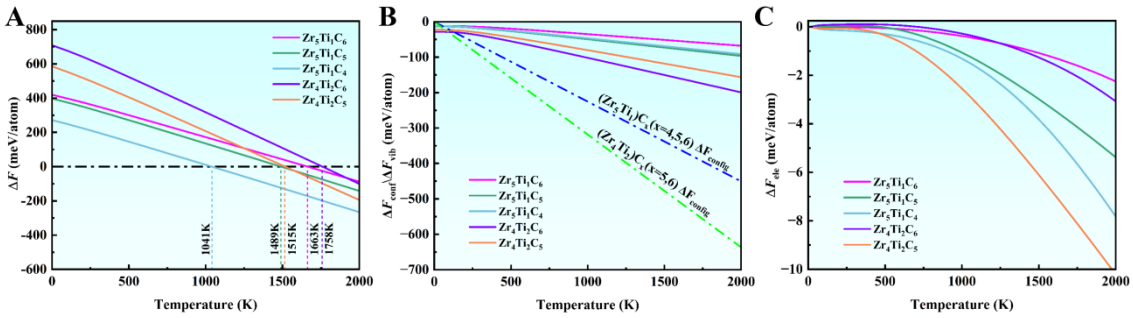

Figure 7. Free energy changes associated with the formation of single-phase (Zr, Ti)C_x solid solution from binary ZrC_x and TiC_x. (A) Helmholtz free energy change (ΔF); (B) Contributions from vibrational (ΔF_{vib}) and configurational (ΔF_{conf}); (C) Electronic free energy change (ΔF_{ele}).

Intrinsically, the single-phase formation ability of multi-component carbides is governed by the mixing enthalpy (ΔH) between their constituent binary carbides (i.e., the total energy difference at 0 K), along with three free energy contributions: configurational (ΔF_{conf}), vibrational (ΔF_{vib}), and electronic (ΔF_{ele}) free energy changes. To further elucidate the single-phase formability of multi-component carbides, Figure 7 presents the individual contributions to the free energy change. C vacancies significantly reduce the ΔH, but the Ti addition increases it. Meanwhile, increased Ti content raises ΔF_{conf}, ΔF_{vib}, and ΔF_{ele} (Figure 7B and C), thereby favoring a reduction in the total free energy (Figure 7A). Comparative analysis shows that ΔH and ΔF_{conf} dominate, with contributions far exceeding those of ΔF_{ele} and ΔF_{vib}. These results indicate that in multi-component carbide systems, the competition between mixing enthalpy and entropy (ΔF_{conf}, ΔF_{vib}, and ΔF_{ele}) collectively determines the temperature range for forming single-phase solid solution and the magnitude of thermodynamic driving force. This conclusion not only validates the reliability of computational approach but also provides a theoretical basis for the rational design and optimization of non-stoichiometric multi-component carbides.

CONCLUSIONS

The present work systematically investigated the thermodynamic stability and elastic properties of binary (ZrC, Zr_6C_5, Zr_3C_2) and ternary ($Zr_5Ti_1C_6$, $Zr_5Ti_1C_5$, $Zr_5Ti_1C_4$, $Zr_4Ti_2C_6$, $Zr_4Ti_2C_5$) carbides using first principles calculations. The main findings are summarized as follows:

(i) Based on the cluster-plus-glue-atom model representing the local CSROs of elemental distribution, the cluster structural unit of MC-type carbides was identified as [C-M_6](C,□)$_5$ (M = Zr/Ti, □ = vacancy), where vacancies occupy the glue atom sites along with C atoms. A 12-atom periodic supercell structure was then used as the input for the first principles calculations. The results demonstrate that introducing C vacancies reduces both the formation energy and free energy at HTs, thereby enhancing thermodynamic stability of FCC carbides. In contrast, Ti substitution for base Zr increases both energy terms, reducing stability. The variation in free energy is mainly governed by entropy contributions: C vacancies significantly raise the vibrational, electronic, and configurational entropies, lowering the free energy. Ti alloying, however, reduces the dominant vibrational entropy, leading to a net increase in free energy. Owing to the synergistic effect of C vacancies and Ti alloying, the [C-Zr_5Ti_1](C,□)$_5$ (=$Zr_5Ti_1C_5$) carbide exhibits the lowest formation energy and free energy among all compositions studied, indicating exceptional thermodynamic stability.

(ii) Analysis of the electronic and vibrational density of states was performed to elucidate the factors governing carbide stability. The phonon spectra confirm the dynamic stability of all modeled carbides, as no imaginary frequencies are present. C vacancies enhance the low-frequency phonon contribution, whereas Ti substitution shifts phonon states to higher frequencies due to its lower atomic mass. Changes in elastic properties are closely linked to electronic structure: both vacancies and Ti addition weaken the covalent-type TDOS peaks in the total density of states, reducing M-C bond strength, which in turn leads to increased binding energy and decreased Young's modulus.

(iii) The single-phase formability of multi-component carbides was also evaluated. Results indicate that C vacancies significantly lower the synthesis temperature required to form single-phase FCC solid solution in (Zr, Ti)-C carbides from binary precursors, thereby improving the single-phase formability. This is attributed to the reduced mixing enthalpy in vacancy-containing carbides. Conversely, increasing Ti content raises the mixing enthalpy and synthesis temperature, making it more challenging to achieve single-phase solid solutions in multi-component (Zr, Ti)-C systems. Therefore, in (Zr, Ti)-C carbides, introducing an appropriate concentration of carbon vacancies while

maintaining a higher content of Zr rather than Ti is of great importance for the high-temperature stability of materials in extremely high-temperature applications.

DECLARATIONS

Authors' contributions

Made substantial contributions to conception and design of the study and performed data analysis and interpretation: Zhang QX, Niu B, Wang Q, Zhang ZW;

Performed data acquisition, as well as provided administrative, technical, and material support: Li Z, Dong C.

Availability of data and materials

The data that support the findings of this study are available from the corresponding author upon reasonable request.

Financial support and sponsorship

None.

Conflicts of interest

Chuang Dong is an Associate Editor of the journal *Journal of Materials Informatics*, but was not involved in any steps of editorial processing, notably including reviewer selection, manuscript handling, and decision making, while the other authors have declared that they have no conflicts of interest.

Ethical approval and consent to participate

Not applicable.

Consent for publication

Not applicable.

REFERENCES

1. Wyatt, B. C.; Nemani, S. K; Hilmas, G. E.; Opila, E. J.; Anasori, B. Ultra-high

temperature ceramics for extreme environments. *Nat. Rev. Mater*. **2023**, *9*, 773-789. DOI: 10.1038/s41578-023-00619-0

2. Xiang, H.; Xing, Y.; Dai, F.; et al. High-entropy ceramics: Present status, challenges, and a look forward. *J. Adv. Ceram.* **2021**, *10*, 385-441. DOI: 10.1007/s40145-021-0477-y

3. Shojaie-bahaabad, M.; Bozorg, M.; Najafizadeh, M; et al. Ultra high temperature ceramic coatings in thermal protection systems (TPS). *Ceram. Int.* **2024**, *50*, 9937-9951. DOI: 10.1016/j.ceramint.2023.12.372

4. Lun, H. L.; Zeng, Y.; Xiong, X.; et al. Oxidation Behavior of Non-Stoichiometric (Zr,Hf,Ti)Cx Carbide Solid Solution Powders in Air. *J. Adv. Ceram.* **2021**, 10, 741-57. DOI: 10.1007/s40145-021-0469-y

5. Harrington, T.J.; Gild, J.; Sarker, P.; et al. Phase stability and mechanical properties of novel high entropy transition metal carbides. *Acta. Mater.* **2019**, *166*, 271-280. DOI: 10.1016/j.actamat.2018.12.054

6. Wang, X. G.; Guo, W. M.; Kan, Y. M.; Zhang, G. J.; Wang, P. L. Densification behavior and properties of hot-pressed ZrC ceramics with Zr and graphite additives. *J. Eur. Ceram. Soc.* **2011**, *31*, 1103-1111.

7. Yang, Q. Q.; Wang, X. G.; Bao, W. C.; et al. Influence of equiatomic Zr/(Ti,Nb) substitution on microstructure and ultra-high strength of (Ti,Zr,Nb)C medium-entropy ceramics at 1900ºC, *J. Adv. Ceram.* **2022**, *11*, 1457-1465. DOI: 10.1007/s40145-022-0623-1

8. Huang, S. S.; Dai, F. F.; Xiang, X. P.; et al. Strengthening or softening: On the impact of off-stoichiometry on the mechanical properties of ZrC. *Acta Mater.* **2025**, *289*, 120892. DOI: 10.1016/j.actamat.2025.120892

9. Dai, F. Z.; Sun, Y. J.; Ren, Y. X.; Xiang, H. M.; Zhou, Y. C. Segregation of solute atoms in ZrC grain boundaries and their effects on grain boundary strengths, *J. Mater. Sci. Technol.* **2022**, *101*, 234-241. DOI: 10.1016/j.jmst.2021.05.058

10. Hossain, M. D.; Borman, T.; Oses, C.; et al. Entropy Landscaping of High-Entropy Carbides. *Adv. Mater.* **2021**, *33*, 2102904. DOI: 10.1002/adma.202102904

11. He, L.; Liu, L.; Peng, F.; et al. Host lattice and solid solution formation in an octal-cation (NbTaZrTiHfVWMo)C high entropy carbide ceramic. *J. Eur. Ceram. Soc.* **2023**, *43*, 5792-5801. DOI: 10.1016/j.jeurceramsoc.2023.06.061

12. Deadmore, D. L. Vaporization of Tantalum Carbide-Hafnium Carbide Solid Solutions.

J. Am. Ceram. Soc. **2010**, *48*, 357-359. DOI: 10.1111/j.1151-2916.1965.tb14760.x

13. Han, X. X.; Girman, V; Sedlak, R; et al. Improved creep resistance of high entropy transition metal carbides. *J. Eur. Ceram. Soc.* **2020**, *40*, 2709-2715. DOI: 10.1016/j.jeurceramsoc.2019.12.036

14. Ye, B. L.; Wen, T. Q.; Huang, K. H.; Wang, C. Z.; Chu, Y. H. First-principles study, fabrication, and characterization of $(Hf_{0.2}Zr_{0.2}Ta_{0.2}Nb_{0.2}Ti_{0.2})C$ high-entropy ceramic. *J. Am. Ceram. Soc.* **2019**, *102*, 4344-4352. DOI: 10.1111/jace.16295

15. Zeng, Y.; Wang, D.; Xiong, X.; et al. Ablation-resistant carbide $Zr_{0.8}Ti_{0.2}C_{0.74}B_{0.26}$ for oxidizing environments up to 3,000 ºC. *Nat. Commun.* **2017**, *8*, 15836. DOI: 10.1038/ncomms15836

16. Sheindlin, M.; Falyakhov, T.; Petukhov, S.; Valyano, G.; Vasin, A. Recent advances in the study of high-temperature behaviour of non-stoichiometric TaC_x, HfC_x and ZrC_x carbides in the domain of their congruent melting point. *Adv. Appl. Ceram.* **2018**, *117*, s48-s55. DOI: 10.1080/17436753.2018.1510819

17. Liu, D.; Hou, Y.; Meng, J.; Zhang, A.; Han, J.; Zhang, J. The significant influence of carbon content on mechanical and thermal properties of $(VNbTaMoW)_{0.5}C_x$ high entropy carbides. *J. Eur. Ceram. Soc.* **2022**, *42*, 5262-5272. DOI: 10.1016/j.jeurceramsoc.2022.06.073

18. Schmid, B.; Koutná, N.; Ntemou, E. Mechanical properties of VC/ZrC and VC/HfC superlattices. *Acta Mater.* **2024**, *270*, 119852. DOI: 10.1016/j.actamat.2024.119852

19. Wang, Z.; Yu, Z.; Zhang, L.; et al. Tailoring structural, mechanical, and electronic properties of $(Ti_{0.25}Ta_{0.25}Zr_{0.25}Nb_{0.25}$-La $)C$ high-entropy carbide ceramics via rare-earth La incorporation: A comprehensive first-principles study. *Ceram. Int.* **2025**, *51*, 33721-33730. DOI: 10.1016/j.ceramint.2025.05.107

20. Chen, L.; Kong, Q.; Liu, Q.; et al. Covalent bonds enhancing and microstructure evolution induced by carbon content in multi-component (TiZrNbMo)C ceramics. *J. Materiomics*, **2025**. *11*, 101048. DOI: 10.1016/j.jmat.2025.101048

21. Zhang, Y.; Liu, B.; Wang, J. M.; Wang, J. Y. Theoretical investigations of the effects of ordered carbon vacancies in ZrC_{1-x} on phase stability and thermo-mechanical properties. *Acta Mater.* **2016**, *111*, 232-241. DOI: 10.1016/j.actamat.2016.03.074

22. Zunger, A.; Wei, S.; Ferreira, L. G.; Bernard, J. E. Special quasirandom structures. *Phys. Rev. Lett.* **1990**, *65*, 353-356. DOI: 10.1103/PhysRevLett.65.353

23. Kim, J. First-principles investigation of the elastic properties and phase stability of $(Ti_{1-x}Ni_x)C_{1-y}$ ternary metastable carbides. *J. Alloy. Compd.* **2021**, *853*, 157349. DOI:

10.1016/j.jallcom.2020.157349

24. Liu, S. Y.; Qin, L,; Zhang H. L.; et al. Design of superhard high-entropy diborides via high-throughput DFT and thermodynamics calculations. *Ceram. Int.* **2024**, *50*, 17977-17987. DOI: 10.1016/j.ceramint.2024.02.287

25. Liu, S. Y.; Zhang, S. X.; Liu, S. Y. Stability and mechanical properties of single-phase quinary high-entropy metal carbides: First-principles theory and thermodynamics. *J. Eur. Ceram. Soc.* **2022**, *42*, 3089-3098. DOI: 10.1016/j.jeurceramsoc.2022.02.034

26. Liu, Y.; Lu, Y.; Yi, W.; et al. Effects of solutes on thermodynamic properties of (TMZrU)C (TM = Ta, Y) medium-entropy carbides: a first-principles study. *J. Mater. Inf.* **2023**, *3*, 17. DOI: 10.20517/jmi.2023.19

27. Meng, H.; Chu, Y. Surface energies in high-entropy carbides with variable carbon stoichiometry. *J. Am. Ceram. Soc.* **2022**, *105*, 5835-5842. DOI: 10.1111/jace.18521

28. Ma, Y.; Wang, Q.; Jiang, B. B.; et al. Controlled formation of coherent cuboidal nanoprecipitates in body-centered cubic high-entropy alloys based on $Al_2(Ni,Co,Fe,Cr)_{14}$ compositions. *Acta Mater.* **2018**, *147*, 213-225. DOI: 10.1016/j.actamat.2018.01.050

29. Yuan, J. H.; Li, Z.; Yang, Y. J.; et al. Applications of machine learning method in high-performance materials design: a review. *J. Mater. Inf.* **2024**, *4*. 14. DOI: 10.20517/jmi.2024.15

30. Wang, W. Y.; Shang, S. L.; Wang, Y.; et al. Atomic and electronic basis for the serrations of refractory high-entropy alloys. *npj Comput. Mater.* **2017**, *3*, 23. DOI: 10.1038/s41524-017-0024-0

31. Bie, X. H.; Hou, J.; Zhou, X.; Song, J. Sub-stoichiometry and vacancy structures in V/Nb carbide precipitates by cluster expansion and first-principles calculations. *Acta Mater.* **2024**, *269*, 119806. DOI: 10.1016/j.actamat.2024.119806

32. Hu, W. T.; Xiang, J. Y.; Zhang, Y.; et al. Superstructural nanodomains of ordered carbon vacancies in nonstoichiometric $ZrC_{0.61}$. *J. Mater. Res.* **2012**, *27*, 1230-1236. DOI: 10.1557/jmr.2012.72

33. Gusev, A. I. Phase equilibria, phases and chemical compounds in the Ti-C system, *Russ. Chem. Rev.* **2002**, 71, 439-463.DOI:10.1070/RC2002v071n06ABEH000721

34. Gusev, A. I.; Rempel, A. A. Order-Disorder Phase Transition Channel in Niobium Carbide. *Phys. Status Solidi A.* **1986**, *93*, 620219. DOI: 10.1002/pssa.2210930108

35. Xiang, J. Y.; Hu, W. T.; Liu, S. C.; et al. Spark plasma sintering of the nonstoichiometric ultrafine-grained titanium carbides with nano superstructural domains

of the ordered carbon vacancies. *Mater. Chem. Phys.* **2011**, *130*, 352-360. DOI: 10.1016/j.matchemphys.2011.06.048

36. Hong, Q. J.; Van De Walle, A. Prediction of the material with highest known melting point from ab initio molecular dynamics calculations. *Phys. Rev. B.* **2015**, *92*, 020104. DOI: 10.1103/PhysRevB.92.020104

37. Gusev, A. I.; Rempel, A. A. Superstructures of non-stoichiometric interstitial compounds and the distribution functions of interstitial atoms. *Phys. Status Solidi*. **1993**, *135*, 15-58. DOI: 10.1002/pssa.2211350102

38. Zeng, Y.; Xiong, X.; Li, G. D.; Chen, Z. K.; Sun, W.; Wang, D. N. Microstructure and ablation behavior of carbon/carbon composites infiltrated with Zr-Ti. *Carbon*. **2013**, *54*, 300-309. DOI: 10.1016/j.carbon.2012.11.042

39. Kresse, G.; Furthmuller, J. Efficiency of ab-initio total energy calculations for metals and semiconductors using a plane-wave basis set. *Comp. Mater. Sci.* **1996**, *6*, 15-50. DOI: 10.1016/0927-0256(96)00008-0

40. Kresse, G.; Furthmuller, J. Efficient iterative schemes for ab initio total-energy calculations using a plane-wave basis set. *Phys. Rev. B.* **1996**, *54*, 11169-11186. DOI: 10.1103/PhysRevB.54.11169

41. Kresse, G.; Joubert, D. From ultrasoft pseudopotentials to the projector augmented-wave method. *Phys. Rev. B.* **1999**, *59*, 1758-1775. DOI: 10.1103/PhysRevB.59.1758

42. Perdew, J. P.; Burke, K.; Ernzerhof, M. Generalized gradient approximation made simple. *Phys. Rev. Lett*. **1996**, *77*, 3865-3868.DOI: 10.1103/PhysRevLett.77.3865

43. Momma, K.; Izumi, F. VESTA 3 for three-dimensional visualization of crystal, volumetric and morphology data. *J. Appl. Crystallogr.* **2011**, *44*, 1272-1276. DOI: 10.1107/S0021889811038970

44. Wang, V.; Xu, N.; Liu, J. C.; Tang, G.; Geng, W. T. VASPKIT: A user-friendly interface facilitating high-throughput computing and analysis using VASP code. *Comput. Phys. Commun.* **2021**, 267, 108033. DOI: 10.1016/j.cpc.2021.108033

45. Grimme, S.; Ehrlich, S; Goerigk, L. Effect of the damping function in dispersion functional theory. *J. Comput. Chem.* **2011**, *32*. 1456-1465. DOI: 10.1002/jcc.21759

46. Ma, D., Grabowski, B., Körmann, F., Neugebauer, J.; Raabe, D. Ab initio thermodynamics of the CoCrFeMnNi high entropy alloy: Importance of entropy contributions beyond the configurational one. *Acta Mater.* **2015**. *100*, 90-97. DOI: 10.1016/j.actamat.2015.08.050

47. Togo, A.; Tanaka, I. First principles phonon calculations in materials science. *Scr.*

Mater. **2015**, *108*, 1-5. DOI: 10.1016/j.scriptamat.2015.07.021

48. Togo, A.; Chaput, L.; Tanaka, I.; Hug, G. First-principles phonon calculations of thermal expansion in Ti_3SiC_2, Ti_3AlC_2, and Ti_3GeC_2, *Phys. Rev. B.* **2010**. *81*, 174301. DOI: 10.1103/PhysRevB.81.174301

49. Olsson, P. A. T.; Blomqvist, J.; Bjerkén, C.; Massih, A. R. Ab initio thermodynamics investigation of titanium hydrides. *Comput. Mater. Sci.* **2015**, *97*, 263-275. DOI: 10.1016/j.commatsci.2014.10.029

50. Ye, B. L.; Wen, T. Q.; Nguyen, M. C.; Hao, L. Y.; Wang, C. Z.; Chu, Y. H. First-principles study, fabrication and characterization of $(Zr_{0.25}Nb_{0.25}Ti_{0.25}V_{0.25})C$ high-entropy ceramics. *Acta Mater.* **2019**. *170*, 15-23. DOI: 10.1016/j.actamat.2019.03.021

51. Le Page, Y.; Saxe, P. Symmetry-general least-squares extraction of elastic data for strained materials from ab initio calculations of stress. *Phys. Rev. B.* **2002**, *65*, 104104. DOI: 10.1103/PhysRevB.65.104104

52. Wu, X. F.; Vanderbilt, D.; Hamann, D. R. Systematic treatment of displacements, strains, and electric fields in density-functional perturbation theory. *Phys. Rev. B.* **2005**, *72*, 035105. DOI: 10.1103/PhysRevB.72.035105

53. Zakarian, D.; Khachatrian, A.; Firstov, S. Universal temperature dependence of Young's modulus, *Met. Powder Rep.* **2019**, *74*, 4, 204-206. DOI: 10.1016/j.mprp.2018.12.079

54. Réjasse, F.; Trolliard, G.; Léchelle, J. Study of the TiC_{1-x}-TiO_2 reactive interface. *Acta Mater.* **2018**, *146*, 225-236. DOI: 10.1016/j.actamat.2017.12.055

55. Luo, Z. L.; Du, Y.; Mao, H. Phase field simulation of the lamellar precipitation in the TiC-ZrC system. *Ceram. Int.* **2018**, *44*, 22041-22044. DOI: 10.1016/j.ceramint.2018.08.299

56. Lei, J. F.; Okimura, H.; Brittain, J. O. The electrical resistance of the group IV transition metal monocarbides and mononitrides in the temperature range 20-1000 °C. *Mater. Sci. Eng. A.* **1990**, *123*, 129-140. DOI: 10.1016/0921-5093(90)90218-R

57. Mahday, A. A.; El-Eskandarany, M. S.; Ahmed, H. A.; Amer, A. A. Mechanically induced solid state carburization for fabrication of nanocrystalline ZrC refractory material powder. *J. Alloy. Compd.* **2000**, *299*, 244-253. DOI: 10.1016/S0925-8388(99)00679-9

58. Sara, V. R. The System Zirconium—Carbon. *J. Am. Ceram. Soc.* **1965**. *48*, 243-247. DOI: 10.1111/j.1151-2916.1965.tb14729.x

59. Zhou, Y.; Watts, J.; Li, C.; Fahrenholtz, W. G.; Hilmas, G. E. Vacancy ordering in zirconium carbide with different carbon contents. *J. Eur. Ceram. Soc.* **2023**. *43*, 5814-5821. DOI: 10.1016/j.jeurceramsoc.2023.05.044.

60. Lun, H. L.; Yuan, J. H.; Zeng, Y.; Xiong, X.; Wang, Q.; Ye, Z. M. Mechanisms responsible for enhancing low-temperature oxidation resistance of nonstoichiometric (Zr,Ti)C. *J. Am. Ceram. Soc.* **2022**, *105*, 5309-5324. DOI: 10.1111/jace.18479

61. Lu, W. Y.; Xu, J. R.; Huang, S. S.; Xiang, X. P.; et al. The coupling of carbon non-stoichiometry and short-range order in governing mechanical properties of high-entropy ceramics. *npj Comput. Mater.* **2025**. *11*, 64. DOI: 10.1038/s41524-025-01551-3

62. Kim, H.; Kim, M.; Kim, J.; Kim, J. Enhancing the hydrogen storage properties of (Ti, M)C_{1-x} materials (M = W, Mg, Ni, and Al) depends on the carbon vacancies: Potential for the recycling of scraps. *Int. J. Refract. Met. Hard Mater.* **2024**. *118*, 106475. DOI: 10.1016/j.ijrmhm.2023.106475

63. Baranov, V. M.; Knyazev, V. I.; Korostin, O.S. The temperature dependence of the elastic constants of nonstoichiometric zirconium carbides. *Strength Mater.* **1973**, *5*, 1074-1077. DOI: 10.1007/BF00762754

64. Sangiovanni, D.; Tasnádi, F.; Harrington, T.; Odén, M.; Vecchio, K; Abrikosov, I. Temperature-dependent elastic properties of binary and multi-component high-entropy refractory carbides. *Mater. Des.* **2021**. *204*, 109634. DOI: 10.1016/j.matdes.2021.109634

65. Evitts, L.; Middleburgh, S.; Kardoulaki, E.; Ipatova, I.; Rushton, M.; Lee, W. Influence of boron isotope ratio on the thermal conductivity of uranium diboride (UB_2) and zirconium diboride (ZrB_2). *J. Nucl. Mater.* **2020**, *528*, 151892. DOI: 10.1016/j.jnucmat.2019.151892

66. Esters, M; Oses, C; Hicks, D; et al. Settling the matter of the role of vibrations in the stability of high-entropy carbides. *Nat. Commun.* **2021**, *12*, 5747 DOI:10.1038/s41467-021-25979-5.

67. Markström, A.; Andersson, D.; Frisk, K. Combined ab-initio and experimental assessment of $A_{1-x}B_xC$ mixed carbides. *Calphad.* **2008**, *32*, 615-623. DOI: 10.1016/j. calphad.2008.07.014.

68. Razumovskiy, V. I.; Ruban, A. V.; Odqvist, J.; Dilner, D.; Korzhavyi, P. A. Effect of carbon vacancies on thermodynamic properties of TiC-ZrC mixed carbides. *Calphad*. **2014**, *46*, 87-91. DOI: 10.1016/j.calphad.2014.02.005

Supplementary Materials

Supplementary Table 1. The basic information of $MC/M_6C_5/M_6C_4$ solid solution structural input unit for first principles calculation constructed by cluster-plus-glue-atom model.

		x (α)	y (β)	z (γ)
Basic Vector		$\sqrt{6}/2a_0$	$\sqrt{6}/2a_0$	$\sqrt{6}/2a_0$
Angle		60°	109.47°	99.59°
Atomic Positions	Central atom of cluster	0.00	0.00	0.00
	Shell atoms of cluster	0.25	0.00	0.75
		0.75	0.00	0.25
		0.25	0.33	0.08
		0.25	0.67	0.42
		0.75	0.67	0.92
		0.75	0.33	0.58
	Glue atoms of cluster	0.50	0.00	0.50
		0.00	0.33	0.33
	M_6C_4 vacancy	0.50	0.33	0.83
	M_6C_4 vacancy	0.50	0.67	0.17
	M_6C_5 vacancy	0.00	0.67	0.67

Supplementary Table 2. The formation and binding energy for TiC, Ti_6C_5 and Ti_3C_2 carbides.

Composition	**Formation energy (eV/atom)**	**Binding energy (eV/atom)**
TiC	-0.750	-7.516
Ti_6C_5	-0.776	-7.429
Ti_3C_2	-0.725	-7.244

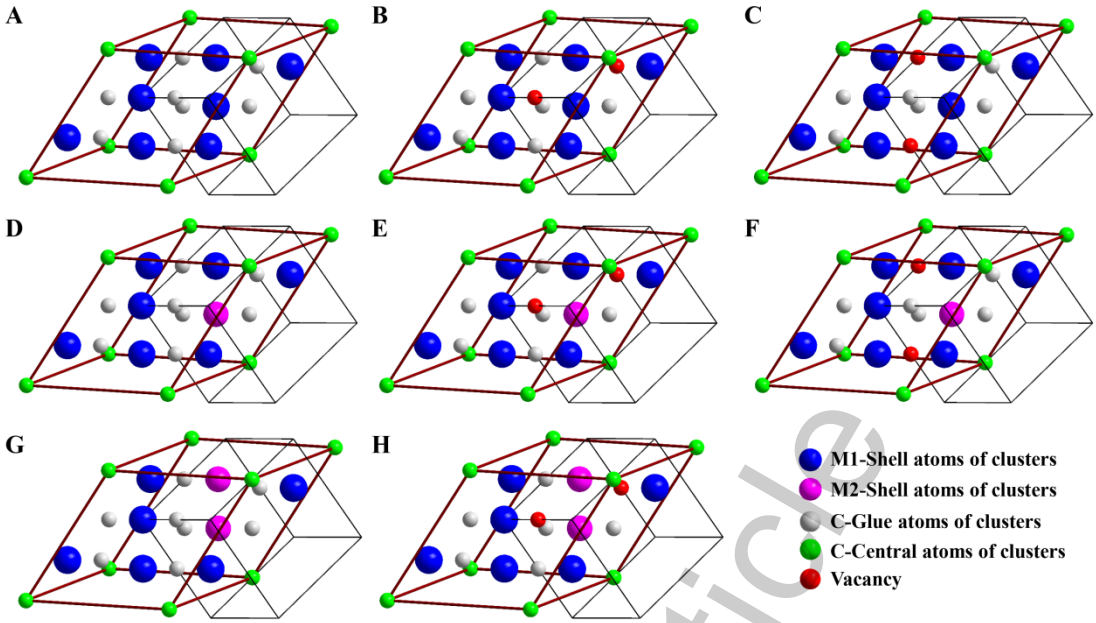

Supplementary Figure 1. Specific cluster structural models of $[C\text{-}M_6](C,\square)_5$ (M = Zr/Ti, □ = vacancy) as inputs for first-principles calculations. (A) M_6C_6; (B) M_6C_5; (B) M_3C_2; (D) $M1_5M2_1C_6$; (E) $M1_5M2_1C_5$; (F) $M1_5M2_1C_4$; (G) $M1_4M2_2C_6$; (H) $M1_4M2_2C_5$. Blue, pink, gray, green, and red spheres represent M1 (shell atoms of clusters), M2 (shell atoms of clusters), C (glue atoms of clusters), C (central atoms of clusters), and vacancies, respectively.

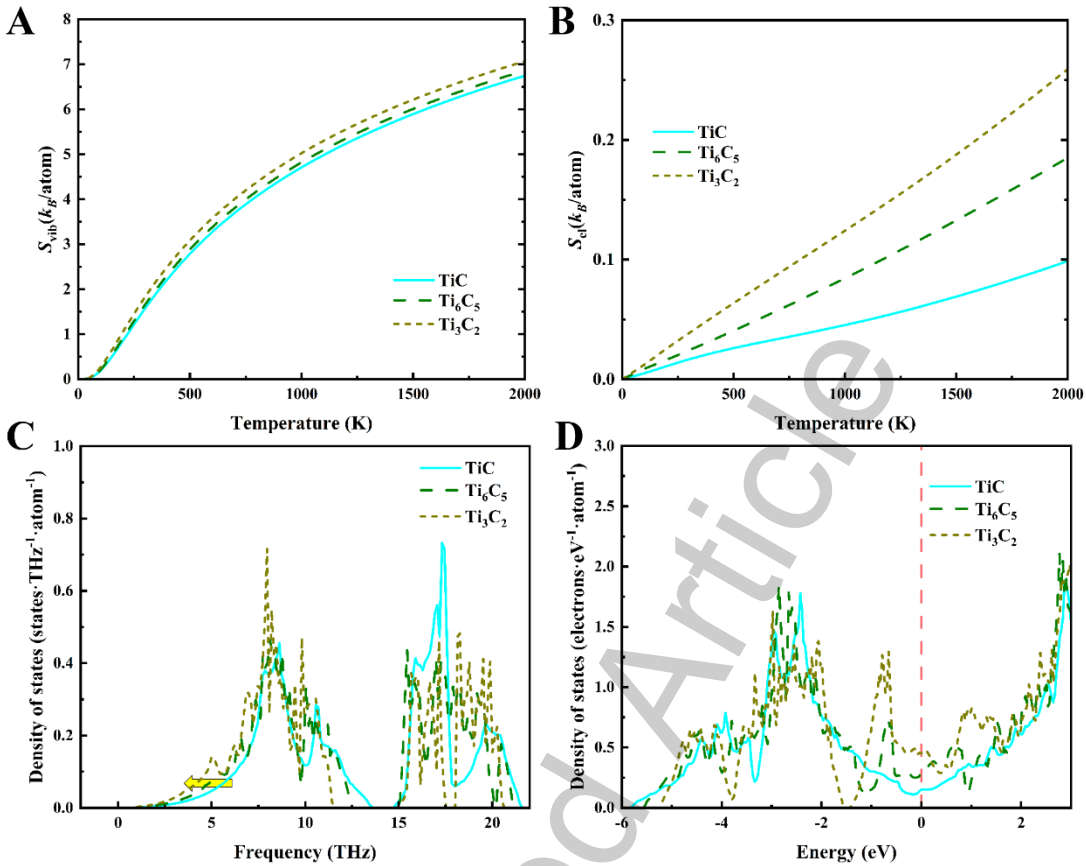

Supplementary Figure 2. Entropy contributions and density of states analysis for TiC_x carbides. (A) Vibrational entropy; (B) Electronic entropy; (C) Phonon density of states; (D) Electronic density of states.

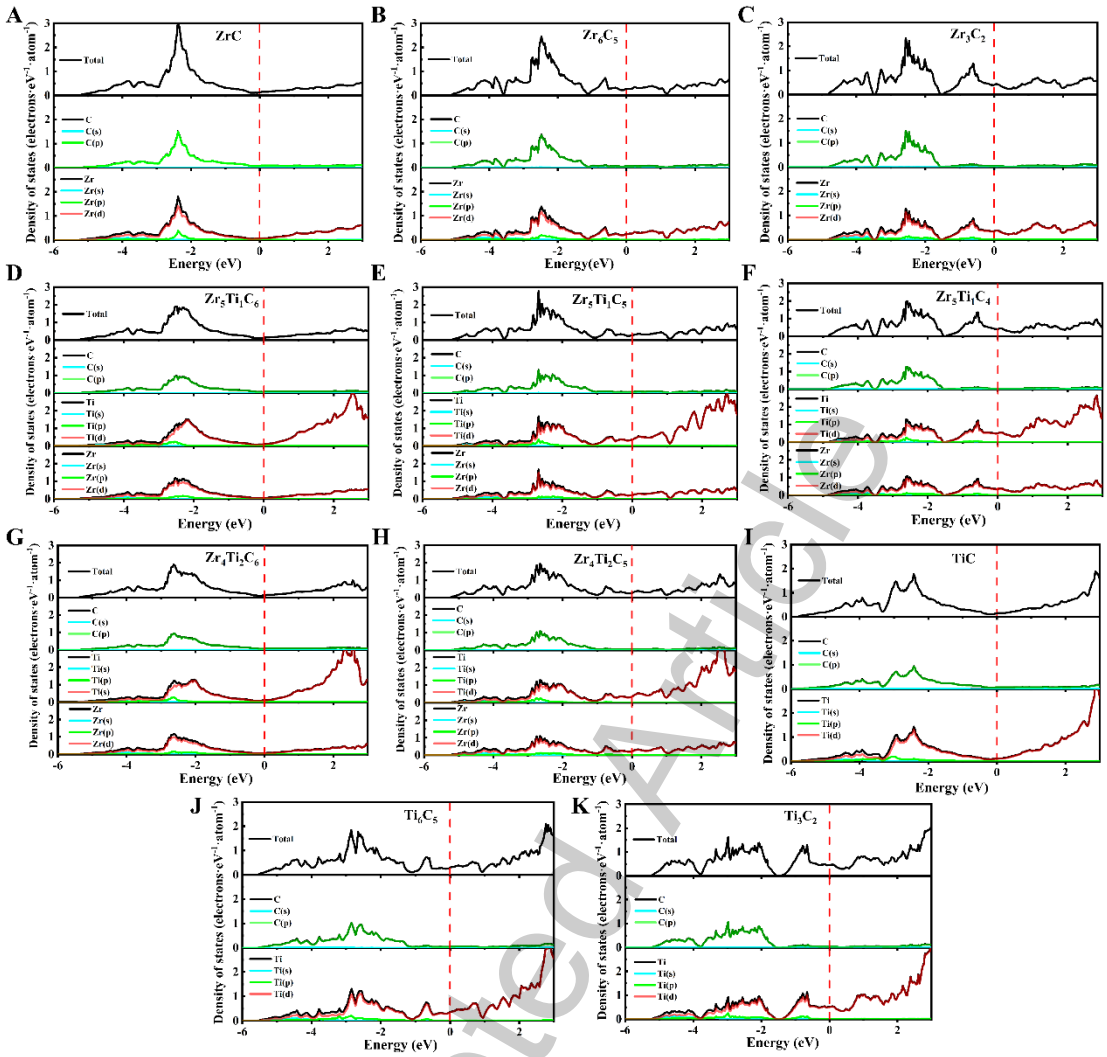

Supplementary Figure 3. Electronic density of states for (Zr, Ti)C_x carbides. (A) ZrC; (B) Zr_6C_5; (C) Zr_3C_2; (D) $Zr_5Ti_1C_6$; (E) $Zr_5Ti_1C_5$; (F) $Zr_5Ti_1C_4$; (G) $Zr_4Ti_2C_6$; (H) $Zr_4Ti_2C_5$; (I) TiC; (J) Ti_6C_5; (K) Ti_3C_2. Vertical read dotted line denotes as the Fermi level.

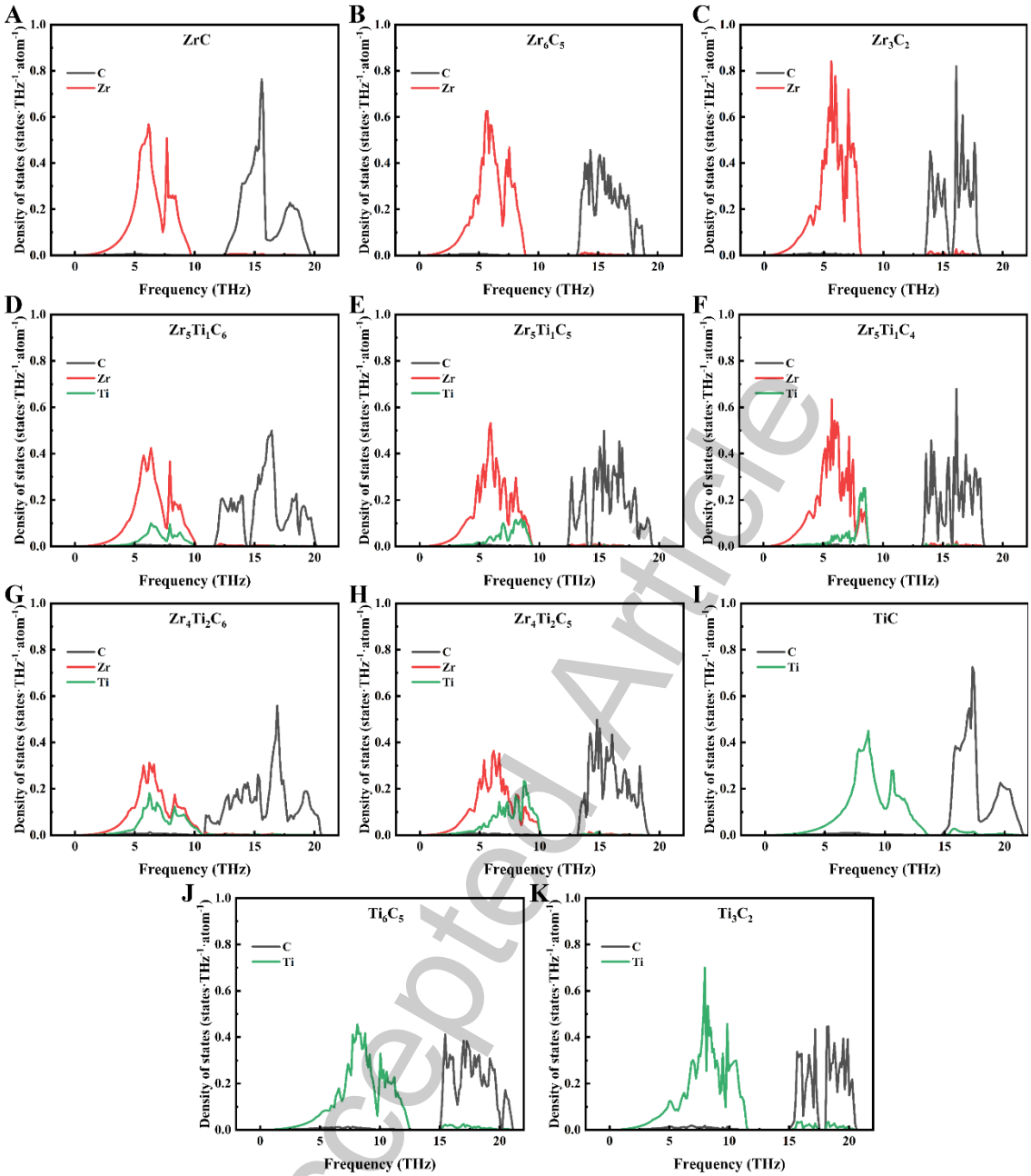

Supplementary Figure 4. Element-projected phonon density of states for (Zr, Ti)C_x carbides. (A) ZrC; (B) Zr_6C_5; (C) Zr_3C_2; (D) $Zr_5Ti_1C_6$; (E) $Zr_5Ti_1C_5$; (F) $Zr_5Ti_1C_4$; (G) $Zr_4Ti_2C_6$; (H) $Zr_4Ti_2C_5$; (I) TiC; (J) Ti_6C_5; (K) Ti_3C_2.